J. Synchrotron Rad. (1998). **5**, 1250–1257

High-Focusing Bragg-Crystal Polychromator Design for Energy-Dispersive X-ray Absorption Spectroscopy

J. Pellicer-Porres,[a]† A. San Miguel[a]*‡ and A. Fontaine[b]

[a]*European Synchrotron Radiation Facility, BP 220, F-38043 Grenoble CEDEX, France, and* [b]*Laboratoire de Magnétisme Louis Néel, CNRS, BP 166, F-38042 Grenoble CEDEX, France. E-mail: sanmigue@dpm.univ-lyon1.fr*

(*Received 12 September 1997; accepted 10 March 1998*)

The design of a highly focusing profiled Si(111) Bragg crystal polychromator for dispersive EXAFS (extended X-ray absorption fine structure) experiments is described. The contour of the crystal has been optimized to give the best focus over the full 4–13 keV energy range. The profile optimization has been improved taking into account all the degrees of freedom of the geometry and the results of X-ray tracing simulations. The profile of the crystal has been calculated to take full advantage of the new possibilities given by the undulator source and the optics of beamline ID24 at the European Synchrotron Radiation Facility. Full spot sizes have been measured to be between 20 and 40 μm in the 5–12 keV energy range. These values compare well with X-ray tracing simulations and are the smallest spots ever obtained with energy-dispersive EXAFS optics, keeping, however, a wide enough energy bandpass for most X-ray absorption spectroscopy experiments.

Keywords: EXAFS; focusing; polychromators; X-ray optics.

1. Introduction

X-ray absorption in dispersive mode (DXAS) collects in parallel all the data of XAS (X-ray absorption spectroscopy) spectra over a large spectral range (Matsushita & Phyzackerly, 1981; Flank *et al.*, 1983). This scheme is based on dispersive optics, *i.e.* a bent perfect crystal which reflects a polychromatic beam out of a white source. After being focused at the sample position, the photons are collected by a position-sensitive detector able to work under high-flux conditions (Tolentino *et al.*, 1988, 1990; Koch *et al.*, 1996). The energy–direction correlation given by the crystal polychromator is transformed into an energy–position correlation at the detector position. Since all the data of a spectrum are acquired simultaneously, the time resolution achievable is in the millisecond range. In addition, since no mechanical movement takes place during the data collection, the stability of this experimental set-up is excellent. These characteristics of the spectrometer are of interest mainly for time-resolved and X-ray magnetic circular dichroism experiments. High-pressure experiments using diamond anvil cells also take advantage of the high quality of the focus of the DXAS instrument (Itié *et al.*, 1992). In that case the small size and the homogeneity of the focus are essential parameters. Consequently, such a focus is required for aberration-free optics. At other synchrotron facilities, up to now, the best achievement of focus sizes on a DXAS spectrometer range from 500 to 100 μm. The reduction of the focus size with the optics described in this paper has allowed the study of smaller samples and consequently opens up new types of experiments. In particular, we can cite the first XAS experiment over megabar pressures (San Miguel, Polian *et al.*, 1998), the first results on EXAFS on single crystals at high pressure (Itié *et al.*, 1997), the development of nanosecond-resolved XMCD experiments (Bonfim *et al.*, 1997; Pizzini *et al.*, 1998) or an energy-dispersive microXANES experiment (Mosbah *et al.*, 1998). Examples of reference data are given elsewhere (Hagelstein *et al.*, 1997).

This paper describes the design and the commissioning of a Bragg-contoured polychromator crystal which achieves a focus size between 20 and 40 μm over the 5–12 keV energy range.

In DXAS experiments the crystal polychromator can be set either in transmission geometry (Laue case) or in reflection geometry (Bragg case). In our energetic range, as shown by Hagelstein *et al.* (1995), the Bragg geometry is much more convenient.

The most commonly used technique to achieve a desired bending of the crystal polychromator in DXAS experiments has been to apply a force to the apex of a triangular-shaped crystal whose base is clamped (Tolentino *et al.*, 1988). The resulting cylindrical shape differs from the ideal elliptical profile (Tolentino *et al.*, 1990) and it gives an aberration proportional to the square of the illuminated

† Present address: Institut de Ciència dels Materials, Universitat de València, Dr. Moliner 50, Ed. Investigació, E-46100 Burjassot, València, Spain. E-mail: julio.pellicer@uv.es.
‡ Present address: Département de Physique des Matériaux, Batiment 203, Université Lyon I, 43 Bd du 11 novembre 1918, F 69622 Villeurbanne, France.

length of the crystal (Ice & Sparks, 1984). To achieve the elliptical profile the curvature has to be increased from the base to the apex of the crystal. This is accomplished by tailoring its width, which no longer varies linearly (Tolentino *et al.*, 1990). However, as one end of the crystal must remain fixed, a different contour is needed, ideally for each energy. This may be too expensive and not too practical. An improvement of this method yields additional degrees of freedom. It consists of using contoured rectangular crystals mounted on four-point benders, which permit almost independent adjustment of two moments (*i.e.* two curvatures) at two points near each end of the crystal (Allen *et al.*, 1993). This is the principle that we have applied. In addition, we have performed more detailed simulations in order to optimize the contour of the crystal to average the minimization of the spot size over the whole 4–13 keV energy domain.

Therefore we computed the crystal elastic behaviour and performed X-ray tracing simulations in order to find the more effective contour to produce the best focus in the 4–13 keV energy domain. Consistent with the theoretical investigation, the smallest spot ever obtained in an energy-dispersive EXAFS spectrometer has been achieved. The optimized bender and the profiling procedure of the polychromator using X-ray tracing is described in the following sections before the presentation of the results of the experimental tests.

2. Theory

To decide the contour of a crystal suited to yield ellipse-induced focusing, we need to choose the medium diffracted energy (E_o) and to set the appropriate geometrical factors of the spectrometer.

To find the best-fitted contour for a crystal polychromator working in the 4–13 keV energy domain, we proceed *via* two steps. First, some geometrical parameters are chosen and the appropriate contoured crystals are calculated for different energies (optimization energies, E_o). Second, the focusing performance of each of these calculated crystals is simulated for other energies (hereafter called calculation energies, E_c) chosen over the 4–13 keV range. This is performed by looking for the best moments that must be applied to the crystal to simulate the new ellipse through a defined figure of merit. The geometrical parameters and the results are compared through this figure of merit. X-ray tracing is used to verify the correctness of the figure of merit and to try to predict the spot size at the focus.

2.1. *Geometrical considerations*

We define a reference frame (x,y) having its origin in the central point (P) of the bent crystal (Fig. 1). The X-ray source (S) and the sample position (I) define the ellipse that the symmetric crystal polychromator must follow in order to attain focusing aberration-free behaviour. In this reference frame, the shape of the ellipse can be expressed as (see, for example, Howells & Lunt, 1993)

$$y = a_2(x^2 + a_3x^3 + a_4x^4 + \ldots), \tag{1}$$

where a_2, a_3 and a_4 are geometrical coefficients depending on the source-to-crystal distance (p), the crystal-to-focus distance (q) and the Bragg angle (θ_B) at the centre of the crystal. Equation (1) is a good approximation when the radius of curvature of the crystal is larger than its length, as in the present case. As the direction of diffraction of the X-rays depends on the angle between the incident rays and the planes of diffraction, the evaluation of the quality of approximation (1) is given by the differences between the slope derived from (1) and that of the exact formula of the ellipse (the figure of merit, defined later, is based on this calculation). This difference is less than 1%.

Keeping only the first term in (1), the basic equations of cylindrical optics remain, *i.e.*

$$1/p + 1/q = 2/R\sin\theta_B, \tag{2}$$

where R is the radius of curvature of the crystal at P. Equation (2) defines the energy bandpass, given by

$$\Delta E = E\cot g\theta_B(l/R - l\sin\theta_B/p). \tag{3}$$

The use of an undulator source, as is the case in ID24, can introduce an additional limitation in the energy bandpass. In most of the cases, this can be avoided by tapering the undulator and/or using the even harmonics of the undulator source (see Hagelstein *et al.*, 1997).

In the absence of optical aberrations, the energy resolution of the polychromator (Tolentino *et al.*, 1988) depends on the spatial resolution of the detector, the size of the X-ray source, the penetration depth of the incident X-rays into the bent crystal, and the intrinsic Darwin width of the

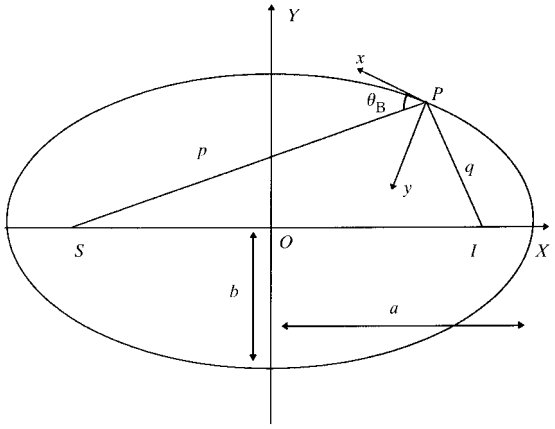

Figure 1
The X-ray source, S, and the focus point, I (polychromatic image), are located at the two focuses of the ellipse. a and b are the half-axis lengths. The curved polychromator is centred at point P. p is the source-to-crystal distance and q is the crystal-to-polychromatic focus distance. θ_B is the Bragg angle. The two coordinate systems (x,y) and (X,Y) described in the text are explicitly shown. At the energy-dispersive XAS beamline at the ESRF (ID24), p = 29.7 m and q can be adjusted from 0.5 to 1.5 m. Obviously the figure is not drawn to scale.

rocking curve of the perfect crystal. The two latter factors deal with the polychromator optics. For a fixed curvature radius of the crystal, the only way to increase the energy resolution will be to increase the Miller indices of the diffraction planes. Nevertheless, the ultimate limiting factor of the energy resolution in XAS experiments is a given fraction of the core-hole width of the probed atom. A good compromise between energy resolution and energy bandpass, in the energy domain under consideration, is obtained with an Si(111) reflection. As explained by Tolentino *et al.* (1988), the contribution of the source is minimized if the crystal-to-sample distance, q, is approximately equal to the sample-to-detector distance, d. The resolution decreases slowly if $d > q$ (but the decrease is negligible for small X-ray sources as the undulators at ESRF beamlines) and increases very fast if $d < q$. Consequently we will set $d \geq q$.

Aberrations can contribute to losses in the energy resolution that can be of the order of the core-hole width. Then, any correction of the aberration should improve the energy–position correlation. It is easy to see from the size of the spot which we have measured with the profiled crystal that the remaining aberrations introduce losses of energy resolution smaller than the core-hole width.

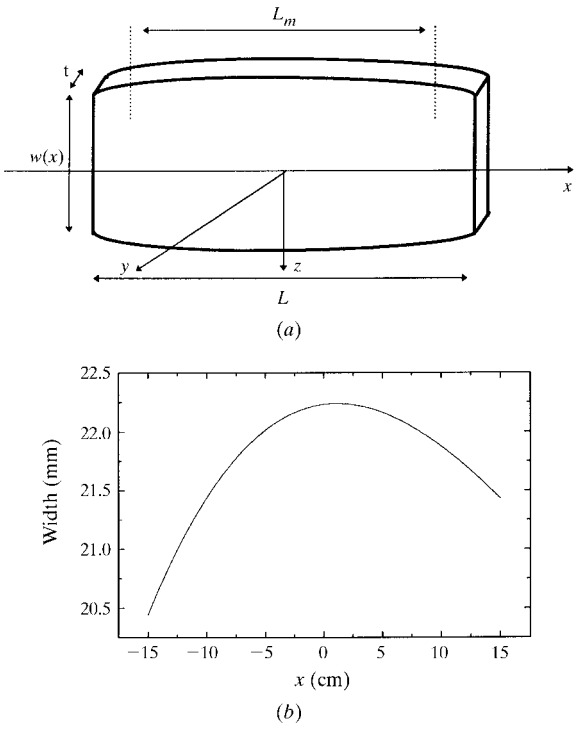

Figure 2
(*a*) Description of the contoured crystal. L, t and w are the crystal length, thickness and width, respectively. L_m is the distance between the points where the moments are applied with the four-point bender. The typical values of these parameters in our experiment are L = 300 mm, t = 1 mm, $w(x) \simeq$ 21.5 mm and L_m = 260 mm. (*b*) Profile of the crystal as described by equation (6) with the optimization energy chosen at 7 keV and a q value of 0.8 m. The width contour is not symmetric as expected in order to be able to produce an elliptical bending.

2.2. *Elastic behaviour and crystal profile*

The elastic equation of a beam bent at two points is (see, for example, Landau & Lifschitz, 1986)

$$E_{\rm Y} I \frac{{\rm d}^2 y}{{\rm d}x^2} = \frac{M_1 + M_0}{2} + \frac{M_1 - M_0}{2} \frac{x}{L_m}, \qquad (4)$$

where $E_{\rm Y}$ is the Young modulus in the compression/dilatation direction, *i.e.* the x direction in Fig. 2(*a*). The right-hand side of (4) describes the distribution of internal moments along the beam. M_0 and M_1 are the internal moments at the points of application of the external forces, which are separated by a distance L_m. The curvature of the crystal is approximated by the second derivative of y with respect to x. I is the section moment around the neutral axis, and is given by $I = wt^3/12$.

Equation (4) is valid for small flexures (the radius of curvature of the beam is large compared with its length) and if the external forces are concentrated at discrete points of the beam, as is the case with a four-point bender.

From (4) one realizes that an x-dependent moment, $I(x)$, enables one to design the real variable curvature along the crystal close to the ideal one. This can be performed by varying either the thickness or, with better control, the width of the crystal. Such a width variation required to obtain a crystal with the elliptic curvature is given by

$$w(x) = \frac{3(M_1 + M_0)}{E_{\rm Y} t^3 a_2} \frac{1 + \frac{2(M_1 - M_0)}{M_1 + M_0} \frac{x}{L_m}}{1 + 3a_3 x + 6a_4 x^2}. \qquad (5)$$

Any pair of moments M_0 and M_1 can be used to calculate the crystal profile. However, to move as little as possible away from the unprofiled crystal (rectangular), we choose, following Underwood (1977), the M_0 and M_1 values that approximate better the rectangular crystal to the ellipse. By introducing these moments in (5) we obtain the profile of the crystal (see Fig. 2*b*) optimized for the diffracting energy E_o of the central point P.

2.3. *Evaluation of the crystal behaviour at new energies*

This is the second step of the evaluation before executing the profile cutting. For each crystal contour given by the first iteration we calculate its performances at other energies E_c of the central point. Other energies imply other Bragg angles and consequently other ellipses rotated and translated with respect to the first one.

Under new moments, the crystal with the width given by (5) will take a shape given by (4). It is valuable to estimate how large the deviation is from the ideal conditions in order to obtain an energy range of acceptance. The solution of the differential equation gives rise to a system of equations that may be solved numerically.

To compare the ideal ellipse at energy E_c with the shape given by the curved crystal, a figure of merit, Σ, based on the slope comparison of both shapes, is required (since diffraction behaviour is our concern), where

$$\Sigma = \sum_i \left(\frac{\frac{dY_{exact}}{dX}|_i - \frac{dY_{approx}}{dX}|_i}{\frac{dY_{exact}}{dX}|_i} \right)^2 . \quad (6)$$

Equation (6) must be evaluated taking into account that (i) the crystal must be rotated by an angle $\theta_B - \theta_B'$, (ii) the derivatives must be taken in the appropriate reference system, and (iii) a careful choice of the points of comparison is requested (for approximated ellipses the X-rays coming from the source do not impinge on the crystal at the same point as in the case of an exact ellipse).

We look for the best curvatures at the calculation energy E_c to approach the ideal ellipse at this energy. To accomplish this in the simulation we minimize numerically the figure of merit.

The procedure that we have presented to calculate the profile at E_o features two iterative steps: firstly, moment determination, and secondly, profile optimization with a fixed moment distribution. Finally the figure of merit is derived by an additional adjustment of the moments imposed at the profile calculated in the second step. A second cycle of iteration could be envisaged. For three reasons it seems to us unreasonable to proceed further in that direction: (i) the computational accuracy is limited by the finite size of the sampling of the crystal; (ii) the initial calculation proceeds with approximations of the ideal ellipse and formula; (iii) the figure of merit which has been chosen is strongly correlated to the focus size, but other parameters contribute to it, *i.e.* the depth of penetration of X-rays in the crystal or the change of position of each individual reflecting point of the surface with respect to the ideal elliptical profile.

2.4. *Choice of parameters*

Here we consider the geometrical parameters for the ID24 DXAS beamline at the European Synchrotron Radiation Facility (ESRF, Grenoble, France). The source-to-crystal distance is p = 29.7 m. The crystal-to-sample distance, q, can be set between 0.7 and 1.5 m. We have the freedom to change q within this range for different photon energies between 4 and 13 keV. Nevertheless, the choice of q results from a compromise between the creation of a large enough energy bandpass and the need to avoid a too large bending of the crystal.

As yielded by (3), the spectral range limitation is critical at low energies. However, using an undulator as the X-ray source means that there is already a limited bandpass at low energy since the emission derives from the undulator first harmonic. At the ESRF, at low energies, a bandpass $\Delta E/E$ = 0.045 matches the undulator bandpass for a typical value of q = 0.8 m. For that q value the energy E_o = 7 keV produces a calculated crystal that optimizes the figure of merit, Σ, for the 4–13 keV range. Fig. 3 shows Σ for crystals contoured for different E_o values with the corresponding experimental q values. Fig. 3 also shows evidence of the presence of a second minima at an energy (E_1) higher than the one (E_o) used for the optimization. The gap between E_o and E_1 increases rapidly with E_o. The iteration process which is used for the profile evaluation is in fact an approximate route to reach the optimized parameters. Therefore, it may be possible that a profile derived from a second step of the iteration could provide us with a slightly better energy dependence of the figure of merit and possibly with a single minima. To attain that kind of accuracy is probably not possible given all the limits inherent to this calculation.

2.5. *X-ray tracing*

Before proceeding with the X-ray tracing we used the multilamellar crystal code in the *XOP* package (Sanchez del Rio *et al.*, 1998) to check that, with the curvatures and the energy range used, no significant asymmetric broadening of the rocking curve occurs with the curved crystal as analysed by Hagelstein *et al.* (1995). The X-ray penetration at the V, Fe, Cu and Ge *K*-edges in the relevant experimental conditions are 2.9, 2.3, 3.5 and 4.3 μm, respectively (determined by the extinction length l_e). Therefore, we can make the simulation by considering the crystal as a mirror. The calculated spot sizes will be then underestimated by a quantity of the order of $l_e \cos\theta_B \sin\theta_B \simeq 1$ μm due to the finite extinction length.

The parameters of the X-ray source of the crystal are obtained by X-ray tracing of the previous elements of the beamline. The effective source observed by the polychromator of the ID24 beamline is located at the focus point of the second mirror of the Kirkpatrick–Baez optics (see Fig. 1 of Hagelstein *et al.*, 1997). This secondary source can be conveniently described by a Gaussian distribution both for the spatial and angular coordinates with parameters σ_x = 100 μm, σ_z = 509 μm, $\sigma_{x'}$ = 410 μrad and $\sigma_{z'}$ = 16 μrad, where x is the demagnification direction and z is the vertical one. Table 1 summarizes the X-ray tracing results for both the profiled crystal optimized at 7 keV and

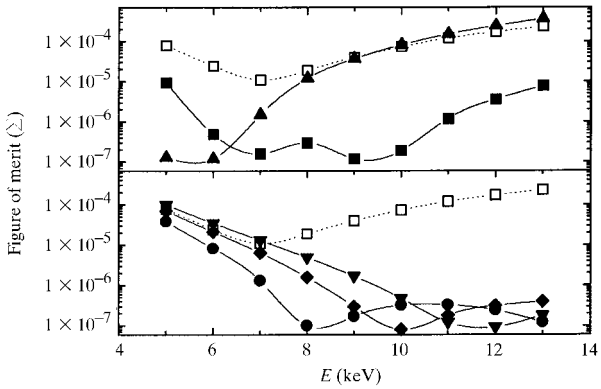

Figure 3
The plot is split into two panels for clarity and shows the energy-dependent figure of merit for crystals profiled for different optimization energies (E_o). This plot shows how a 7 keV value for the optimization energy gives rise to a crystal that minimizes the figure of merit in the energy range 5–12 keV. The figure of merit is shown for profiled crystals with E_o values of 5 keV (filled up-triangles), 7 keV (filled squares), 9 keV (filled circles), 11 keV (filled diamonds) and 13 keV (filled down-triangles) and also for a rectangular crystal (hollow squares).

Table 1
Experimental conditions at the different measured energies.

The crystal-to-focus distance, q, was kept constant at 82 cm for all experiments except at 5.46 keV where it was set to 140 cm. The illuminated size of the crystal (S_c) was set to 20 mm. The table shows the calculated sizes of the focus for an Si(111) profiled crystal optimized at 7 keV and the calculated size of the spot when using a non-profiled crystal. The spot size is the size needed to integrate 90% of the radiation.

E (keV)	5.465	7.112	8.979	11.103
ΔE (eV)	95	300	485	745
q' (mm)	1400	820	820	820
S_c (mm)	20	20	20	20
Spot (μm) (profiled crystal)	30	23	40	25
Spot (μm) (rectangular crystal)	–	30	60	170

the rectangular crystal (non-profiled crystal). The energies chosen for the simulations are the same as those used in the test experiments. The spot size is estimated as the spatial gap containing 90% of the X-rays to ensure we take into account properly the tails of the image spot. The correlation between the spot size and the figure of merit is 0.86.

3. Experience and discussion

For tests performed at the ESRF energy-dispersive XAS beamline (ID24), the crystal is mounted on a specially designed four-point bender that provides independent and opposite couples at two points near each end of the crystal. The crystal is held by cylindrical rollers at only four points, minimizing the strain and consequently the distortions of the crystal lattice. The two couples are computer controlled by step-by-step motors. A motorized twist correction has also been implemented combining a differential screw and a piezoelectric transducer. This actuator restores the cylindrical shape of the reflecting surface. This correction has proved to be essential for obtaining a well defined focus. The heat load on the crystal is partially drained by immersing the bottom third of the crystal in a eutectic Ga–In bath which produces a temperature gradient only in the direction perpendicular to the plane of energy dispersion. The eutectic bath is kept at a constant temperature of 292 K. The beam size on the crystal (S_c) was set with the help of two motorized and cooled copper slits placed just before the polychromator. A complete description of the mechanical part of the system is given elsewhere (San Miguel, Hagelstein *et al.*, 1998).

Two symmetrically cut Si(111) crystals were tested: a profiled crystal (E_o = 7 keV) and one identical but with a rectangular contour.

Three different sets of data were collected to investigate the following:

(*a*) *The focus size at different energies*. The focus size was evaluated using a 7.5 μm-wide slit made of 20 μm-thick molybdenum foils moved by 5 μm steps. We tuned the applied moments to optimize the spot size and the uniformity of the distribution of energies within the spot. Fig. 4 compares the spots obtained with the profiled and the rectangular crystals at three different energies, after deconvoluting them by a 7.5 μm-wide slit function. It is worth noting that the focus distance was kept constant at 820 mm for all the studied energies except for 5.465 keV, for which we had to work under vacuum conditions. At this energy the geometrical constrains imposed by the equipment forced us to work at a distance of 1400 mm. Because of these constraints, the bandpass is reduced for this energy.

Table 2
Summary of experimental conditions and results obtained.

The values of the spot size obtained by X-ray tracing and the calculated value of the figure of merit are also given for comparison. We studied the spot size for the profiled and rectangular crystal, the focus depth and the influence of the illuminated length of the crystal. S_c is the source size; Σ is the figure of merit.

Energy (keV)	q (mm)	S_c (mm)	Σ	Calculated spot size	Measured spot size
Profiled crystal					
5.465	1400	20	1.1×10^{-5}	27	30
7.112	820	20	1.6×10^{-7}	11	23
8.979	820	20	7.9×10^{-7}	9.5	40
11.103	820	20	7.5×10^{-6}	17	25
Rectangular crystal					
7.112	820	20	1×10^{-5}	11.5	30
8.979	820	20	4.1×10^{-5}	35	60
11.103	820	20	1.2×10^{-4}	76	170
Variation of the illuminated length of the crystal					
7.112	820	14	–	9.5	25
7.112	820	10	–	9.5	25
Depth of focus					
7.112	817	20	–	42	55
7.112	818	20	–	22.5	40
7.112	819	20	–	11	25
7.112	820	20	–	11	25
7.112	821	20	–	45	50
7.112	822	20	–	46	55
7.112	823	20	–	70	60

(*b*) *The field depth of the focus*. The focus depth (Fig. 5, Table 2) was measured at the energy of the Fe *K*-edge (7.1 keV) giving a value between 1 and 2 mm. The two-step slope appearing both in the X-ray tracing and in the experiment can be attributed to an aberration of the type sketched in Fig. 5(*b*), and can be caused by an error in the slope of the crystal at its middle point.

(*c*) *The dependence of the spot size with the illuminated length of the crystal*. We optimized the spot size for three different lengths of the footprint of the beam impinging on the crystal (which is the projection of S_c onto the crystal) but we did not observe any significant change in the spot size.

These results, together with the results of the X-ray tracing in the same geometrical conditions, are summarized in Table 2, which also includes the more relevant geometrical parameters.

Fig. 6(*a*) shows the experimental spot sizes for both crystals compared with the computed figure of merit. Both parameters show a similar energy dependence, proving the validity of our choice of the figure of merit. In Fig. 6(*b*) the calculated and measured spot sizes for both crystals are shown. First of all we observe the essential improvement yielded by the profiled crystal with respect to the rectan-

Table 3
Comparison between polychromator designs including the achievement at the ESRF.

S is the source size, *q*/*p* is the demagnification factor, FWHM is the full width at half-maximum of the spot and FS is the full size (90% intensity). It is worthwhile to point out the improvement produced by the present work, which achieves a reduction of FS by an order of magnitude.

Reference	Method used	Source size Demagnification factor	Theoretical size	Experimental size
Tolentino *et al.* (1988)	Profiled triangular crystal	S = 6 mm q/p = 0.046	FWHM = 276 μm	FWHM = 300–500 μm
Lee *et al.* (1994)	Rectangular crystal	S = 350 μm q/p = 0.03	FWHM = 10.5 μm	FWHM = 100–120 μm
Allen *et al.* (1993)	Profiled rectangular crystal	S = 5 mm q/p = 0.03	FWHM = 150 μm	FWHM = 175 μm, FS = 600 μm
This work	Optimized profiled rectangular crystal	S = 235 μm q/p = 0.028	FWHM = 6.5–11 μm	FWHM = 10–17 μm, FS = 20–40 μm

gular crystal. This is especially true at high energies. Secondly it also illustrates the proper optimization energy selection that makes it possible to keep a small spot size for the whole energy range.

Despite the reduction of the focus size obtained with the profiled crystal, we observe that the measured spot sizes are systematically larger than the calculated ones (by a factor of ∼1.8). Different origins have to be envisaged:

(i) An underestimation of the source size. The source characteristics provided by the X-ray tracing are generated by idealized mirrors located upstream in the beamline. In comparison, real slope errors increase the size of the secondary source. The slope errors originate very likely from the deformation of the surface of the first mirror owing to the large thermal load deposited by the undulator X-ray source. This point is strengthened by the fact that the

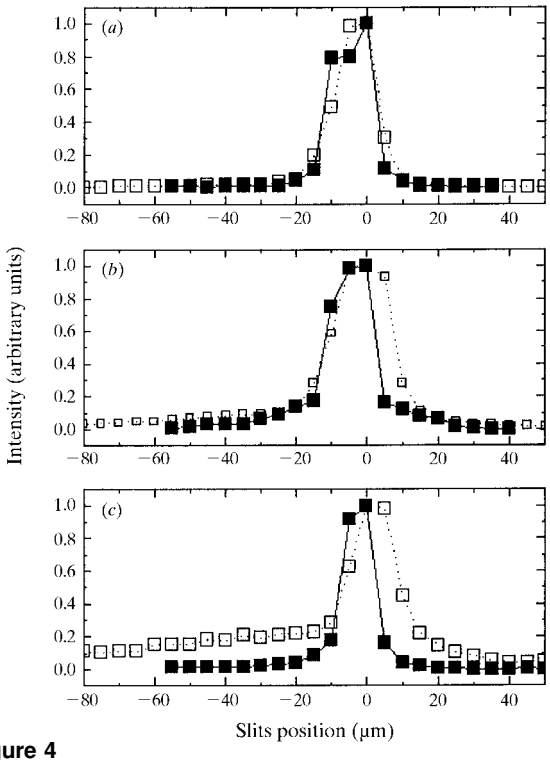

Figure 4
Experimental images of the focus obtained at the beamline with a contoured crystal (filled squares) and with a rectangular crystal (hollow squares). Images (*a*), (*b*) and (*c*) correspond to Bragg-reflected beams centred at the Fe (7.112 keV), Cu (8.979 keV) and Ge (11.103 keV) *K*-edge energies, respectively. These diagrams point out the effectiveness of contour tailoring, especially at high energy.

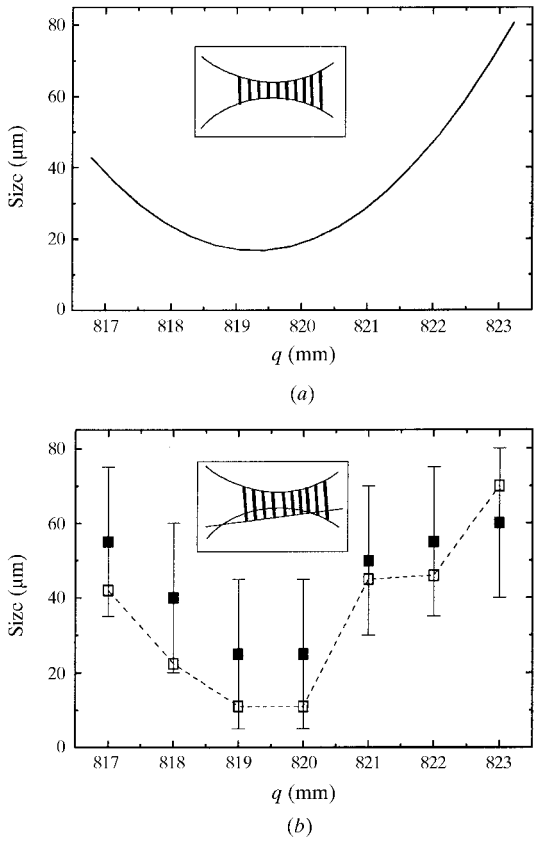

Figure 5
Study of the focus depth. (*a*) The hypothetical focus depth for an optics system without aberrations. The inset represents the horizontal projection of the focus as we cross it. (*b*) The measured focus depth (filled squares) is of the order of 1 mm if the acceptable increase of the image FWHM is limited to 50%. The calculated focus depth (hollow squares) is also shown. The inset shows that the two slopes observed and calculated at each side of the minimum can be explained by involving an aberration.

correlation between the spot size and the figure of merit (that does not depend on the source size) is 0.87, whereas the correlation between the measured size and the calculated size is only 0.7.

(ii) A residual twist in the crystal.

(iii) A variable thickness t of the crystal. If the thickness of the polished crystal is not uniform, the local curvature generated by the bender can fluctuate following the t^{-3} dependence of the moment of inertia. It is easy to understand that a variation $\Delta t = (t/3)(\Delta w/w)$ results in the same ΔI variation as that produced by a variation Δw of the width of the contour. In the present case, the maximum value of $\Delta w/w$ is equivalent to $\Delta t \simeq 20$ μm. The measured thickness error was 10 μm at some points.

(iv) The procedure followed to measure the spot size. With 7.5 μm-wide slits moved in 5 μm steps we are just at the limit for accurate evaluation of image sizes smaller than 30–35 μm (reducing the slit gap leads to too large a sensitivity to artefact effects introduced by coherence). This is clearly appreciated when one takes into account that, with S_c values of 10 and 14 mm, the experimental size is 2.6 times the theoretical one (larger than 1.8, the average factor). Furthermore, in Fig. 6(*b*) it is clearly seen that the ratio between the measured and calculated spot sizes becomes smaller as the spot size increases.

(v) Finally, moving in the other direction, the sharp energy spectrum from the undulator gives a profile of the spot that also looks sharper and this effect is not taken into account in the calculations.

All these sources of errors can also explain that, for the optimizing energy (7 keV), no clear improvement of the focusing has been observed.

It is appropriate to compare the performances of our optics with that of previous works. In Table 3 we have summarized the results obtained by other authors. Full sizes mean that 90% of intensity is included. Specifically it is interesting to look at the results obtained by Allen *et al.* (1993), where using a rectangular profiled crystal they are able to focus a 5 mm-wide source (q/p = 0.03) down to 175 μm FWHM spots, which is 25 μm bigger than the theoretical values. The full size is of the order of 600 μm. In our situation, with rectangular crystals and the optimization of relevant parameters we are able to focus a 235 μm FWHM source (q/p = 0.028) to 10–17 μm FWHM spots, with ideal values of 6.5–11 μm. The full sizes are of the order of 20–40 μm. This achievement of one order of magnitude of reduction in size and a spectacular reduction of the tails of the image, which are the most significant of the aberration figures, is due to the quality of the third-generation source, which, consequently, is very demanding in terms of aberration rejection: the optical aberration to be beaten scales with the ideal image size.

4. Conclusions

We have designed a bent polychromator for energy-dispersive optics that takes advantage of the third-generation synchrotron characteristics. We have investigated the effect of the relevant parameters implemented in an extensive simulation, and have tested experimentally the behaviour of the produced contoured crystal mounted in a four-point bender. Considerable improvements with respect to the rectangular crystal were achieved. Spot sizes as small as 20–40 μm at energies ranging from 5 to 12 keV were measured.

We are grateful to the staff of the ESRF where this work was performed, especially to G. Marot for the bender mechanical design, M. Sanchez Del Rio for his help in the X-ray tracing and M. Hagelstein for his useful comments. One of us (JP) is supported by the Ministerio de Educación y Ciencia of Spain (grant No. PN95 24351836).

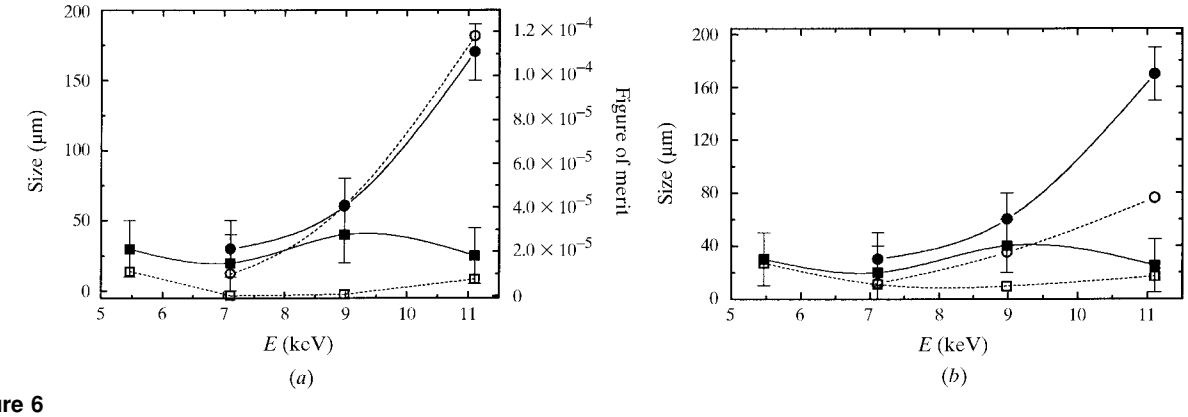

Figure 6
(*a*) Comparison of the experimentally obtained focus size for a contoured crystal (filled squares) and for a rectangular crystal (filled circles) at different photon energies. For comparison, the calculated figure of merit (dotted line, see text for definition) is also shown for the contoured (hollow squares) and rectangular crystal (hollow circles). The lines are just a guide for the eyes. (*b*) Comparison of the calculated and measured focus sizes at different energies for a profiled (squares) and for a rectangular (circles) crystal. The filled squares and circles hold for the measured focus and the hollow squares and circles hold for the calculated focus. The lines are just a guide for the eyes.

References

Allen, P. G., Conradson, S. D. & Penner-Hahn, J. E. (1993). *J. Appl. Cryst.* **26**, 172–179.

Bonfim, M., Mackay, K., Pizzini, S., San Miguel, A., Tolentino, H., Giles, C., Neisius, T., Hagelstein, M., Baudelet, F., Malgrange, C. & Fontaine, A. (1997). *Highlights of the ESRF 1996/1997*, pp. 23–24. ESRF, Grenoble, France.

Flank, A. M., Fontaine, A., Jucha, A., Lemonnier, M., Raoux, D. & Williams, C. (1983). *Nucl. Instrum. Methods*, **208**, 651–654.

Hagelstein, M., Ferrero, C., Hatje, U., Ressler, T. & Metz, W. (1995). *J. Synchrotron Rad.* **2**, 174–180.

Hagelstein, M., San Miguel, A., Fontaine, A. & Goulon, J. (1997). *J. Phys. IV*, **7**(C2), 303–308.

Howells, M. R. & Lunt, D. (1993). *Opt. Eng.* **32**, 1981–1989.

Ice, G. E. & Sparks, C. (1984). *Nucl. Instrum. Methods*, **222**, 121–127.

Itié, J. P., Baudelet, F., Dartyge, E., Fontaine, A., Tolentino, H. & San Miguel, A. (1992). *High Press. Res.* **8**, 697–702.

Itié, J. P., Polian, A., Gauthier, M. & San Miguel, A. (1997). *Highlights of the ESRF 1996/1997*, pp. 57–58. ESRF, Grenoble, France.

Koch, A., Hagelstein, M., San Miguel, A., Fontaine, A. & Ressler, T. (1996). *IS&T/SPIE Proceedings of Symposium on Electronic Imaging: Science and Technology*, San Jose, CA, USA, Vol. 2416, p. 85.

Landau, L. & Lifschitz, E. (1986). *Theory of Elasticity.* Oxford: Pergamon.

Lee, P. L., Beno, M. A., Jennings, G., Ramanathan, M., Knapp, G. S., Huang, K., Bai, J. & Montano, P. A. (1994). *Rev. Sci. Instrum.* **65**, 1–6.

Matsushita, T. & Phyzackerly, R. P. (1981). *Jpn. J. Appl. Phys.* **20**, 2223.

Mosbah, M., Metrich, N., Dura, J. P., San Miguel, A., Delaney, J. S. & Mccammon, C. (1998). In the press.

Pizzini, S., Bonfim, M., Baudelet, F., Tolentino, H., San Miguel, A., Mackay, K., Malgrange, C., Hagelstein, M. & Fontaine, A. (1998). *J. Synchrotron Rad.* **5**, 1298–1303.

Sanchez del Rio, M., Ferrero, C. & Mocella, V. (1998). *Proc. SPIE*, **3151**, 312–323. (http://www.esrf.Fr/computing/expg/subgroups/theory/idl/xop/xop.html.)

San Miguel, A., Hagelstein, M., Borrel, J., Marot, G. & Renier, M. (1998). *J. Synchrotron Rad.* Submitted.

San Miguel, A., Polian, A., Gauthier, H. & Itié, J. P. (1998). In preparation.

Tolentino, H., Baudelet, F., Dartyge, E., Fontaine, A., Lena, A. & Tourillon, G. (1990). *Nucl. Instrum. Methods*, A**289**, 307–316.

Tolentino, H., Dartyge, E., Fontaine, A. & Tourillon, G. (1988). *J. Appl. Cryst.* **21**, 15–21.

Underwood, J. M. (1977). *Space Sci. Instrum.* **3**, 259–270.